ELSEVIER

Contents lists available at ScienceDirect

Acta Materialia

journal homepage: www.elsevier.com/locate/actamat



Full length article

Atomistic simulations of interaction between basal <a> dislocations and three-dimensional twins in magnesium



Mingyu Gong ^a, Guisen Liu ^a, Jian Wang ^{a, b, *}, Laurent Capolungo ^c, Carlos N. Tomé ^c

- ^a Mechanical and Materials Engineering, University of Nebraska-Lincoln, Lincoln, NE, 68588, USA
- b Nebraska Center for Materials and Nanoscience, University of Nebraska-Lincoln, Lincoln, NE, 68588, USA
- ^c MST-8, Los Alamos National Laboratory, Los Alamos, NM, 87544, USA

ARTICLE INFO

Article history:
Received 20 January 2018
Received in revised form
29 May 2018
Accepted 31 May 2018
Available online 14 June 2018

Keywords:
Dislocation
3D twin
Slip transformation
Atomistic simulation

ABSTRACT

Dislocation slip and twinning are equally important in the plastic deformation of hexagonal close packed crystals. Basal slip and extension $\{10\overline{1}2\}$ < $\overline{1}011$ > twins can be activated concurrently in magnesium and, as a result, complex dislocation-dislocation, twin-twin, and dislocation-twin interactions take place and determine the hardening behavior. Here, using atomistic simulations, we study the latter mechanism, namely, the interactions between basal $\langle a \rangle$ dislocations and a three-dimensional (3D) $\{10\overline{1}2\}$ twin. According to our findings, a basal screw dislocation can fully transform into the twin via multiple cross-slip between basal and prismatic planes in the matrix. This process causes the formation of jogs and basal stacking faults in the matrix, and prismatic $\langle a \rangle$ dislocations in the twin. We also find that a basal mixed dislocation cannot directly transform into the twin. Instead, it dissociates into twinning dislocations, resulting in a change in twin thickness and the formation of basal/prismatic steps. When the dislocation interacts with the lateral twin boundary, slip transformation in the twin is accomplished through the gliding of either $\frac{1}{2}$ <a+c> or $\frac{a+c}{2}$ on the prismatic plane in the twin. Accompanying the gliding of $\frac{1}{2} < a + c$, a prismatic stacking fault is created inside the twin. By accounting for the 3D character of the dislocation-twin reactions, our results extend our understanding of slip transformation into a twin, the formation of basal and prismatic stacking faults in matrix and twin, and the role that local stresses and the lateral boundary of the twin play in this process.

 $\ensuremath{\mathbb{C}}$ 2018 Acta Materialia Inc. Published by Elsevier Ltd. All rights reserved.

1. Introduction

Dislocation slip and twinning are equally important in the plastic deformation of hexagonal close packed (hcp) crystals [1–4]. For Mg and Mg alloys, the primary deformation mechanisms at room temperature are basal <a> slip ($\{0001\}<11\overline{2}0>$) and $\{10\overline{1}2\}<\overline{1}011>$ extension twin. Prismatic <a> slip $\{10\overline{1}0\}<11\overline{2}0>$ and pyramidal <a+c> slip $\{11\overline{2}2\}<\overline{11}23>$, are difficult to activate due to the low mobility of the associated dislocations. A considerable amount of work has been devoted to understanding the mechanisms and mechanics of plastic deformation associated with dislocation slip and twins in hexagonal

E-mail address: wangj6@gmail.com (J. Wang).

close packed crystals. The studies regarding dislocations have concentrated on structure, energy, and motion of dislocations, and on their interactions in the framework of dislocation configurations [5–9]. Because basal slip and extension twinning are concurrently activated, complex dislocation-twin [10–27] and twin-twin interactions [28–35], take place and affect strain hardening. In the case of twin-twin interactions, twin-twin boundaries (TTBs) form that subsequently affect the twinning, de-twinning, and slip processes [36–38]. Such mechanism is particularly relevant in connection with cyclic loading [39]. With increasing loading cycles, more TTBs form, and the stability of TTBs requires increasing stresses in order to activate de-twinning, which results in increased strain hardening [32,39].

Although twins are 3-dimensional domains, practically all the work done on dislocation-twin and twin-twin interactions regards the twins as two-dimensional entities, sectioned along the plane that contains the propagation and normal direction [17,18,40–42]. Traditionally, TEM and EBSD studies analyze two-dimensional

^{*} Corresponding author. Mechanical and Materials Engineering, University of Nebraska-Lincoln, Lincoln, NE, 68588, USA.

sections of twins, and only recently results from serial sectioning that capture the volumetric shape of twins in AZ31 Mg have been reported [43]. Also recently, Liu et al. [44] have characterized experimentally and via molecular dynamics method (MD) the structure of the 'lateral' side of $\{10\overline{1}2\}$ twins in Mg. Gong et al. further studied equilibrium and non-equilibrium boundaries associated with 3-D twins by using crystallographic dislocation theory and MD simulations [45]. Luque et al. used MD to study stability of 3D 'terraces' growing on the coherent twin boundary of tensile twins in Mg [46]. We believe that the 3D character of twins has to be accounted for, if one expects to fully understand twintwin interactions, dislocation-twin interactions, and twin transformation across grain boundaries.

In this work, we use as a guide and reference the extensive 2D knowledge acquired in the last half century, and focus on dislocation-twin interactions in Mg from the 3D perspective. We attempt to improve our comprehension about the barriers that twins represent to dislocation glide, the reactions taking place at the twin interfaces, and the characteristics of dislocation transmutation across the twin. Understanding kinetic processes of the slip-twin interactions in hexagonal materials is an indispensable first step for developing a comprehensive understanding of the role that this mechanism plays on hardening the parent and the twin. The majority of experimental studies have concentrated on the interactions between dislocations and coherent twin boundaries in Mg [4,15,20–22], Zn [14,16,47–49], Zr [50–53], and Ti [54]. Wang and Agnew [20] recently conducted a transmission electron microscopy study of dislocation transmutation across twin boundaries, which confirms some previously proposed dislocation transformation reactions, and reveals $\langle c \pm a \rangle$ dislocations in the vicinity of the twin boundary. In addition, geometry models and atomistic simulations have been used for characterizing the interaction of basal <a> dislocation with coherent twin boundary in a 2D framework. The major results can be summarized as follows.

- A screw <a> dislocation can directly transmit across the twin boundary without leaving a residual defect at the twin boundary [13,17,55]. This transmission involves cross-slip of the dislocation from basal plane in the matrix to basal or prismatic plane in the twin.
- A mixed <a> dislocation cannot directly transform across the twin boundary. Instead, the dislocation dissociates into multiple mobile twinning dislocations, resulting in twinning or detwinning with respect to the gliding and formation of PB steps. A residual defect is left at the TB [18,40,41,56-59].
- Two mixed <a> dislocations gliding on a basal plane in the matrix could react to produce one <a+c> dislocation on the prismatic plane in the twin and a residual dislocation at the interface [13,55]. After the reaction, a <a+c> dislocation transforms into the twin via gliding on the prismatic plane of the twin.

The interaction between a dislocation and a boundary depends strongly on the slip systems available in the twin, the atomic structure of the boundary, the local stress state, and temperature [2,22,60–62]. The last two factors can be varied with loading conditions, but the first two factors are determined by the geometrical characteristics of the boundary [18]. Regarding the interaction of a dislocation with a 3D twin, there are two geometric factors. Firstly, besides the widely studied coherent twin boundary and its contribution to twin thickening, there are two other characteristic twin boundaries to consider. One is responsible for the forward ('edge') propagation of the twin domain along the twinning shear direction, while the other is responsible for the lateral

('screw') propagation in a direction perpendicular to the growth and the shear directions. These two twin boundaries are associated with the pileup and rearrangement of twin dislocations (TDs) [45]. Secondly, a dislocation with a given Burgers vector may exhibit screw, edge or mixed character, and may approach the twin from different directions. For example, a basal <a> dislocation line can be parallel to the coherent twin plane, or parallel to the lateral twin boundary. However, knowledge is missing regarding the interactions between a dislocation and lateral twin boundaries, or how a dislocation transforms across a twin domain when it impinges on different sides of the twin.

In this paper, we conduct atomistic simulations of the interaction processes of basal $<\alpha>$ dislocations approaching a three-dimensional (3D) $\{\overline{10}12\}$ twin. In section 2, we describe essential details of simulation models and methods. In section 3, we report on simulation results with respect to the incoming dislocation characters including Burgers vector and line sense and the three twin boundaries. We draw conclusions in section 4. The results provide comprehensive insights of the interactions between a dislocation and a deformation twin.

2. Crystallographic characterization and atomistic simulation

2.1. Crystallographic characterization

In a 3D twin, three types of twin interfaces/facets can be identified, each one related to a different twin propagation direction. For simplicity, a schematic 3D twin domain is presented in Fig. 1, and characteristic boundaries, as identified in experiments and atomistic simulations, are identified. The x-axis coincides with the twin shear direction ($\eta = [10\overline{1}1]$), y-axis is along the twin normal ($\textbf{n} = [\overline{7}078]$) and z-axis is along the lateral direction ($\lambda = [1\overline{2}10]$). The three types of twin boundaries/facets (TBs) are associated with the 'normal' (parallel to n), 'forward' (parallel to η) and 'lateral' (parallel to λ) propagation/growth directions, respectively. The

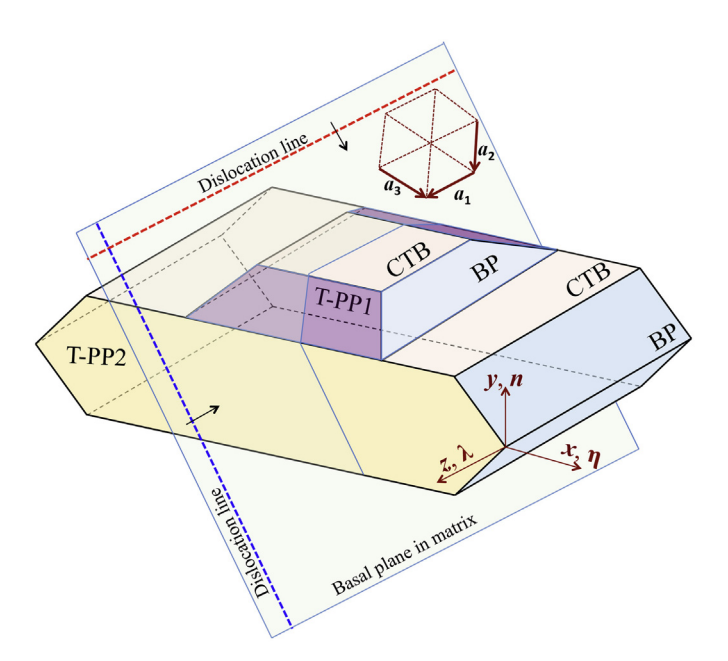


Fig. 1. A schematic three-dimensional twin, showing characteristic boundaries associated with a $\{\overline{1}012\}$ twin and three available basal < a > slip vectors. The red and blue dashed lines denote dislocation lines. The red one is parallel to the z-axis and the blue one is along the < c > axis. The black arrows indicate the moving direction of the dislocation. (For interpretation of the references to colour in this figure legend, the reader is referred to the Web version of this article.)

normal-TB consists mainly of $(\overline{1}012)$ coherent twin boundary (CTB), with serrations consisting of coherent BP/PB steps (the basal plane in the twin or the matrix is parallel to the prismatic plane in the matrix or the twin) associated with the pileup of twinning dislocations (TDs). In 3D the serrations are more likely to become 'terraces' [44-46], as sketched in Fig. 1. The forward-TB forms as a result of the pileup of edge type TDs, showing serrated or faceted structure which contains BP/PB facets [63-67] The lateral-TB forms as a result of the pileup of screw type TDs, and consists of twist prismatic-prismatic (T-PP2) $\{\overline{2}110\} \parallel \{2\overline{11}0\}$ boundaries and twist pyramidal-pyramidal (T-PP1) $\{\overline{1}101\} \parallel \{10\overline{11}\}$ boundaries [44,45]. Notice that the TDs in forward- and lateral-TBs will create local stress fields at the boundaries, which will superpose to the elastic field induced by the shear transformation due to twining. A dislocation approaching a 3-D twin will be subjected to these additional stresses. These local stress fields cannot be studied using the 2D models and atomistic simulations, and it is not known how they affect the dislocation-twin interactions.

Basal <*a*> dislocations have three possible Burgers vectors, $a_1 = [1\overline{2}10]$, $a_2 = [2\overline{11}0]$, and $a_3 = [11\overline{2}0]$, as shown in Fig. 1. The dislocation with a_1 is either screw or edge, depending on whether the dislocation line is either perpendicular to a_1 (blue dashed line) or parallel to a_1 (red dashed line), respectively. With the geometry considered, dislocations with a_2 and a_3 Burgers vectors are of mixed character, with opposite screw component. Thus, the interactions between a_2 or a_3 dislocations and the twin are similar. We studied four possible cases. Case 1: a_1 dislocation approaches the normal-TB. Case 2: a_2 dislocation approaches the normal-TB. Case 3: a_1 dislocation approaches the lateral-TB. The first two cases have been extensively studied under the 2D conditions [17,18,40,41,56–59], while the last two cases have never been studied either for 2D or 3D conditions.

2.2. Molecular dynamics simulations

First, a 3D twin nucleus is created according to the pure-shuffle

nucleation mechanism of $(\overline{1}012)$ twinning [68], at the center of the atomic simulation cell. Following the standard nucleation theory, the nucleus is expected to be coherent [68–70]. This is supported by results showing that below a critical size of approximately 2.8 nm, misfit dislocations are unstable [45,71,72]. Thus, interface energy is first considered when a nucleus forms. Atomistic simulations revealed that the coherent BP/PB interface (97 mJ/m²) has lower interface energy than CTB (130 mJ/m²). Coherent PB and BP boundaries outline a twin nucleus when observed along λ . Since the twin and matrix share the same λ (along the z direction), there is no restriction on the dimension of the twin nucleus along λ (z-axis). The two lateral twin boundaries in the z-direction are coherent prism-prism T-PP2 interfaces, with a low interface energy of 108 mJ/m².

Fig. 2a shows the coherent dichromatic pattern corresponding to pure-shuffle nucleation of a $\{\overline{1}012\}$ twin, and Fig. 2b shows the displacements of atoms inside the twin nucleus. The black symbols and red symbols represent matrix and twin, respectively. The misfit strains, confined to the nucleus by the stiffness of the matrix, are compressive in the $[10\overline{1}0]$ direction (strain -3.15%) and tensile in the [0001] direction (strain 3.36%). Without the formation of misfit dislocations, the dimension of the PB and BP boundaries is 2.8 nm. Since there is no misfit strain along the z-direction, there is no restriction on the dimension along the z-direction. We create one 3D twin nucleus in a $60 \text{ nm} \times 30 \text{ nm} \times 60 \text{ nm}$ single crystal with the x-axis along η direction, y-axis along n direction and z-axis along λ direction. The initial nucleus is shown in Fig. 2c, surrounded by PB, BP, and T-PP2 boundaries. The initial twin structure is relaxed under an applied homogeneous elastic strain at the temperature of 5 K. Fig. 2d and 2e show the growing twin, which is now enclosed by coherent twin boundary (CTB), coherent BP, PB, T-PP1 and T-PP2 boundaries. The twin nucleus grows faster in the λ direction than in the other two directions because of the high mobility of screw-type TDs [73]. The slow propagation of the twin along the twin shear direction η is ascribed to the large PB and BP facets. For the interaction simulations, we start with a relaxed twin nucleus of $20 \text{ nm} \times 10 \text{ nm} \times 20 \text{ nm}$, and the local stress field induced by the relaxation transformation.

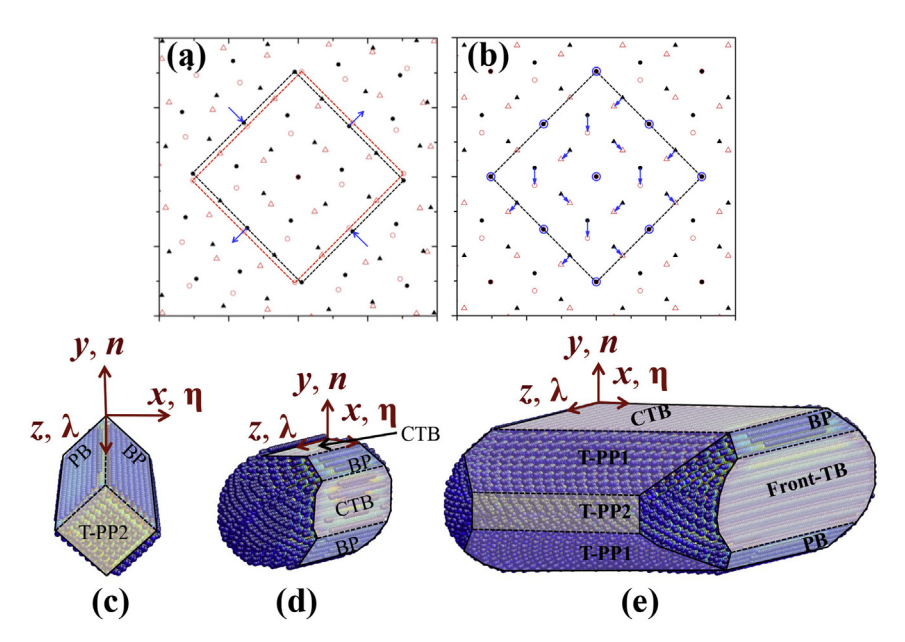


Fig. 2. (a) The coherent dichromatic pattern corresponding to pure-shuffle nucleation of {1012} twin. (b) The displacements of atoms inside the twin. The black symbols and red symbols represent matrix and twin atoms, respectively. (c) The initial twin nucleus in a single crystal, showing PB, BP, and T-PP2 interfaces. (d) and (e) atomic configurations of the twin during growth at different instants, showing several characteristic twin boundaries. (For interpretation of the references to colour in this figure legend, the reader is referred to the Web version of this article.)

A basal $\langle a \rangle$ dislocation is introduced in the model by the application of the anisotropic Barnett-Lothe solutions [74] for the displacement field of a dislocation. This field is applied to both the parent and twin in the first order approximation. Fixed boundary conditions are adopted where atomic positions are fixed within a 1 nm thick layer around the simulation cell. Atomistic simulations were conducted under an applied deformation gradient at temperature of 5 K using the embedded atom method (EAM) potential developed by Liu et al. (referred to as EAM/Liu) [75]. For the case when a mixed basal dislocation approaches the lateral side of a 3D twin, we also conducted a MD simulation with the modified EAM (MEAM/Wu) potential recently developed by Wu et al. [76]. The difference in the transformation phenomenon is ascribed to the structure and energy of prismatic stacking fault which is produced by the two interatomic potentials. The details are discussed in the following section.

3. Atomistic simulations of dislocation-twin interactions

Case 1 An a_1 dislocation (screw type) approaches the normal-TB and the forward-TB.

A pure screw dislocation with the Burgers vector a_1 is introduced into the matrix. The dislocation line on the basal plane is initially 2 nm away from the twin boundary, as shown in Fig. 3a. The model is uniformly deformed by a deformation gradient F_1 .

$$\boldsymbol{F}_1 = \begin{pmatrix} 1 & 0.04 & 0 \\ 0 & 1 & 0 \\ 0.02 & 0.02 & 1 \end{pmatrix}$$

Under the applied deformation gradient, the twin expands in the η and λ directions, while the dislocation moves towards the twin. Fig. 3 shows successive snapshots of the simulations, revealing several novel features. First, before the screw dislocation contacts the normal-TB (or CTB), the interaction between their stress fields make the segment near the twin domain to cross-slip from the initial basal plane onto the prismatic plane (Fig. 3b). The atomic structure inserted in Fig. 3b shows the gliding of the a_1 dislocation on the prismatic plane and three kinks, labeled K_1 , K_1 and K_2 , with length c/2, c/2, and c from left to right. The two K_1 kinks can glide on the prismatic plane, then form a new K_2 kink. As a result, the segment cross-slips on the prismatic plane for two basal interplanar spacings. For convenience in describing

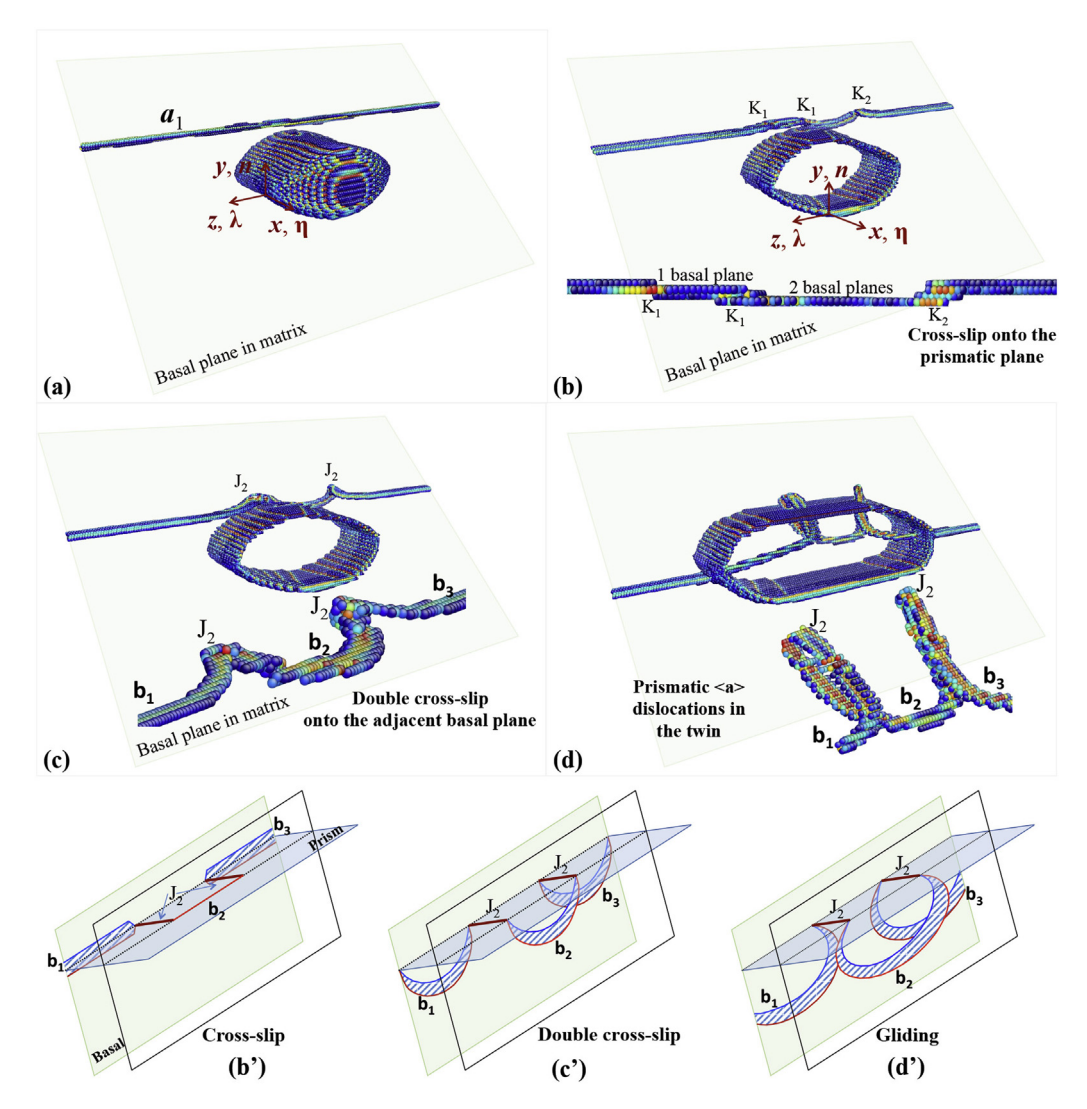


Fig. 3. (a) Initial atomic configuration of case 1 containing a twin and a pure screw a_1 dislocation. (b) First cross-slip of a_1 from basal plane onto prismatic plane, resulting in three kinks, K_1 , K_1 , and K_2 . (c) Double cross-slip of b_2 from prismatic plane onto adjacent basal plane, and the creation of two jogs J_2 accompanying double cross-slip. (d) Transmutation of b_1 , b_2 and b_3 across top twin boundary into the twin. (b'), (c') and (d') Schematics showing the process of first cross-slip, double cross-slip and dislocation transmutation.

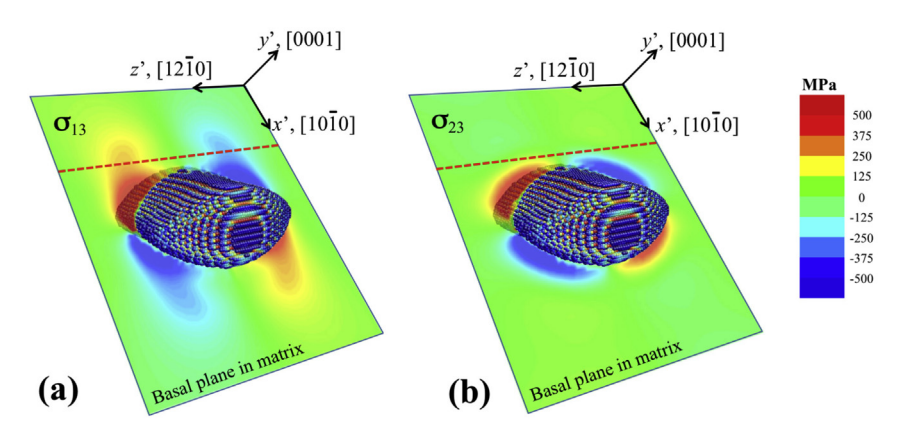


Fig. 4. The stress fields, σ_{13} and σ_{23} , associated with twinning on the glide plane of the a_1 dislocation. The red dashed line indicates the incoming dislocation. (For interpretation of the references to colour in this figure legend, the reader is referred to the Web version of this article.)

dislocation-twin interactions, Fig. 3b' schematically shows the first cross-slip of the dislocation from the basal plane to the prismatic plane. Second, the cross-slip segment (denoted by b₂) crosses again onto the second neighboring basal plane, corresponding to a double cross-slip shown in Fig. 3c and c'. As a consequence, two jogs of length c (denoted by J_2) are created as a result of the double crossslip (the two kinks K₂ are thus called jog), as illustrated in Fig. 3c'. The jogs have Burgers vector a_1 and the line aligns with $\langle c \rangle$. Thus, the jog only glides on the prismatic plane in the matrix but does not move towards the twin. Third, the dislocations gliding on the basal transmit into the twin domain and glide on the prismatic plane as shown in Fig. 3d and d'. Fourth, the jogs pin the dislocations, leaving four prismatic a_1 dislocations in the twin (Fig. 3d). Observe that, in the process, the twin has also grown laterally. As for the parent phase, the interfacial reaction generates four basal a_1 dislocations segments in the matrix, two on the original basal plane and two on the second neighboring basal plane. When the dislocation approaches a PB step on the normal-TB or a BP facet on the forward-TB, a similar process of cross-slip and transformation is observed.

The cross-slip from basal to prismatic planes before slip transformation is attributed to the local deformation gradient and the corresponding stresses near the twin. Fig. 4 shows the stress fields on the glide plane of the a_1 dislocation. For convenience of discussing the cross-slip process, the stresses are described in the crystal reference frame, the x'-axis is along the $[10\overline{1}0]$, the y'-axis is along the [0001] and the z'-axis is along the $[1\overline{2}10]$. According to dislocation theory [77], the Peach-Koehler force produced by the stresses acting on a dislocation line with length dl is:

$$d\mathbf{F} = (\mathbf{b} \cdot \boldsymbol{\sigma}) \times d\mathbf{l}$$

Since the Burgers vector $b = a_1$ is parallel to the dislocation line (along λ), so,

$$m{b} \cdot m{\sigma} = |m{b}| \left(egin{array}{c} \sigma_{13} \ \sigma_{23} \ \sigma_{33} \end{array}
ight)$$

For dl along λ , σ_{23} and σ_{13} are the resolved shears driving the glide of a_1 dislocation on the basal and prismatic planes, respectively. Fig. 4a and b shows the stress fields of σ_{13} and σ_{23} . It is found that σ_{13} has a longer range of influence than σ_{23} , which favors the cross-slip of the dislocation onto the prismatic plane. However, the basal plane is energetically and kinetically preferred for glide. Hence, a double cross-slip occurs, and the dislocation segment crosses again onto the basal plane.

Importantly, the aforementioned reaction products could not be anticipated on the sole basis of crystallographic arguments. The latter would correctly predict the transformation of a basal <*a*> dislocation into a prismatic <*a*> dislocation in the twin domain but would not predict the formation of jogs within the twin domain and the resulting shape of the transformed dislocation that results from pinning. Note that pinning is expected to affect activation of glide in the twin domain because the segment gliding on the prismatic plane will need to overcome the line tension associated with the pinning jogs.

Fig. 5 shows another simulation, where the dislocation impinges on a BP facet instead of a CTB. In addition to the processes observed in Fig. 3, we also observed the glide of jogs on the prismatic plane, as shown in Fig. 5b, 5c and 5d. Differing from the results in Fig. 3, the dislocation entirely transforms across the twin domain without leaving behind prismatic a_1 dislocations (Fig. 5e). This is ascribed to a different process, consistent on four-fold cross-slip, as highlighted in Fig. 5. In order to clearly describe these details, Fig. 6 illustrates the four-fold cross slip, from the original basal plane onto the prismatic plane (1st time), then onto the adjacent basal planes (2nd time), further onto the prismatic plane (3rd time) and finally onto the original basal plane (4th time). As a result, the basal a_1 dislocation transforms into the twin through cross-slipping onto the prismatic plane in the twin. Notice that four jogs J_1 , of length c/2, are created in the process. Four basal a_1 dislocations on the neighboring glide planes are connected by the jogs (Fig. 6c and 6e). Due to the dissociation of basal a_1 dislocations, such a dislocation configuration finally develops a low energy configuration (Fig. 6d and f) with two partial dislocations P_1 and P_2 on each glide plane. These structures are formed in the two J_1 region marked in Fig. 5d and 5e. Theoretically, the dislocation configuration shown in Fig. 6f could not collectively glide along the z-axis, because the P-K forces acting on the two jogs are equal in magnitude but of opposite sign, the same as the P-K forces acting on the partial dislocations dissociated from basal a_1 dislocation on the neighboring glide planes. Since the two shear planes associated with the dissociation of the a_1 are separated by one basal plane, the basal plane between the two glide planes forms a fault structure, as characterized from the corresponding atomic structure in Fig. 6g.

Case 2 An a_2 dislocation approaches the normal-TB.

Fig. 7 shows the transmutation of one a_2 dislocation across the normal-TBs. A mixed dislocation with the Burgers vector a_2 is introduced in the matrix. The dislocation line is parallel to the z-axis, which makes it a mixed 60° basal dislocation. The dislocation

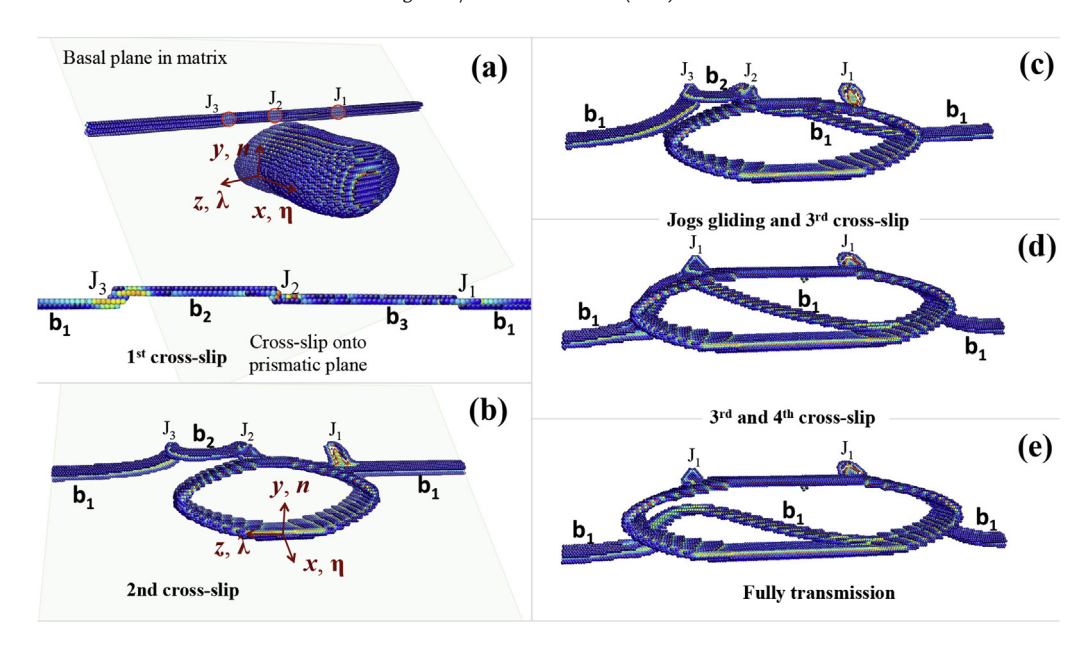


Fig. 5. (a) Initial atomic configuration of case 1' containing a twin and a pure screw a_1 dislocation. Dislocation line undergoes 1st cross-slip and contains three jogs. (b) Snapshot of the 2nd cross-slip. (c) Snapshot shows the glide of jogs together with the 3rd cross-slip. Fault structure forms during cross-slip. (d) Snapshot of 3rd and 4th cross-slip together with formation of another fault structure. (e) Final atomic structure shows the fully transmission of dislocation into twin.

line on the basal plane is initially 2 nm away from the twin boundary, as shown in Fig. 7a. The whole model is uniformly deformed by a deformation gradient F_2 .

$$\mathbf{F}_2 = \begin{pmatrix} 1.02 & 0.04 & 0 \\ 0 & 0.98 & 0 \\ 0 & 0 & 1 \end{pmatrix}$$

Accompanying the relaxation of the applied elastic deformation gradient, the twin propagates in the η and λ directions while the dislocation moves towards the twin. Fig. 7b and 7c reveal several novel features. First, local detwinning takes place (Fig. 7b) associated with the migration of the coherent twin boundary. Second, one BP step of six atomic layers high (Fig. 7b) is created at the interaction site along the normal-TB. This is ascribed to the dissociation of the a_2 dislocation into three twinning dislocations on the twin plane and a residual dislocation. Third, the residual dislocation on the normal-TB is locked and does not transform into the twin (Fig. 7c). The details will be discussed in the following paragraph. Fourth, the rest of the a_2 dislocation continues gliding on the basal plane in the matrix, surrounds the lateral boundary of the twin, and then transforms into the twin from the lateral-TB (Fig. 7c). As a result, prismatic stacking faults (PSFs) are created in the twin, as shown in Fig. 8a. The corresponding slip in the twin is accomplished through the gliding of a $\frac{1}{2}$ < a_1+c_2 dislocation on the prismatic plane. Fifth, the PSFs can be annihilated via the nucleation of a partial loop in the faulted region Fig. 8b and 8c. This will be discussed in the following section (Case 4) in connection with the interaction between a_2 dislocation and the lateral-TB. In addition to the dislocation-twin interaction, we also observed the emission of dislocations on basal plane from the forward-TB (more precisely, at the intersection line between the BP and PB facets) into the matrix (Fig. 7c). This is probably due to the high stress concentration at the BP/PB ridge, which facilities the nucleation and emission of basal dislocations in order to relax the stress concentration [45].

The detwinning and the creation of a BP step are a consequence of the reaction of the incoming dislocation a_2 with the CTB. Such kind of reaction has been reported extensively in the literature. It has been shown that when a mixed dislocation interacts with twin

boundaries, TDs and residual defects are produced at the CTB via the dissociation of the incoming lattice dislocation [41,57,58,78,79]. A TD associated with $\{\overline{1}012\}$ twinning in an hcp crystal is a disconnection (a zonal defect) with dislocation character with Burgers vector b_{TD} and step character with height h [80,81]. Other common elements that describe a unit TD are the twin plane, twinning direction, and scalar twin shear [3]. The detailed energetics and kinetics underlying the reactions at common twin boundaries have been examined via MD simulation [41,57,59,73,78,82-84]. The reaction of a mixed 60 $^{\circ}$ basal dislocation a_2 at the $\{\overline{1}012\}$ twin boundary is given by $\frac{1}{2}[2\overline{11}0](0001) =$ $n\rho[10\overline{1}1](\overline{1}012) + b_r^{(\overline{1}012)}$. This twinning dislocation encompasses two "rumpled" ($\overline{1}012$) planes and has a Burgers vector $\boldsymbol{b}_{TD}^{(\overline{1}012)} =$ $\rho[10\overline{1}1]$, where ρ varies with the ratio c/a and corresponds to 1/15 for Mg [72]. The number n indicates the population of twinning dislocations that could be dissociated from the mixed 60° basal dislocation. The largest n may be close to 5 for Mg. In our simulations *n* turns out to be 3, corresponding to a six atomic-layer PB step associated with the pileup of three TDs. Accompanying the glide of TDs along the TBs, the CTB migrates upwards or downwards depending on the side of the interaction site (see Fig. 9), expanding or contracting the twin domain in the process. A similar process is also observed when the a_2 dislocation approaches the PB or BP steps, including the larger PB or BP facets associated with the forward-TB. The results are comparable to the two-dimensional simulations [57,59,73,78,79,83,84] except for the interaction with the lateral-TB.

Case 3 An a_1 dislocation approaches the lateral-TB

When the line of an a_1 dislocation in Fig. 10a is parallel to $[10\overline{1}0]$ on the basal plane, the dislocation is a pure edge type and does not cross slip onto the prismatic plane. The dislocation is initially placed 3 nm away from the lateral-TB. Under the applied deformation gradient F_1 , the dislocation fully transforms across the twin without leaving a residual defect on the twin boundary (Fig. 10b). The transformation is accomplished through the gliding of the a_1

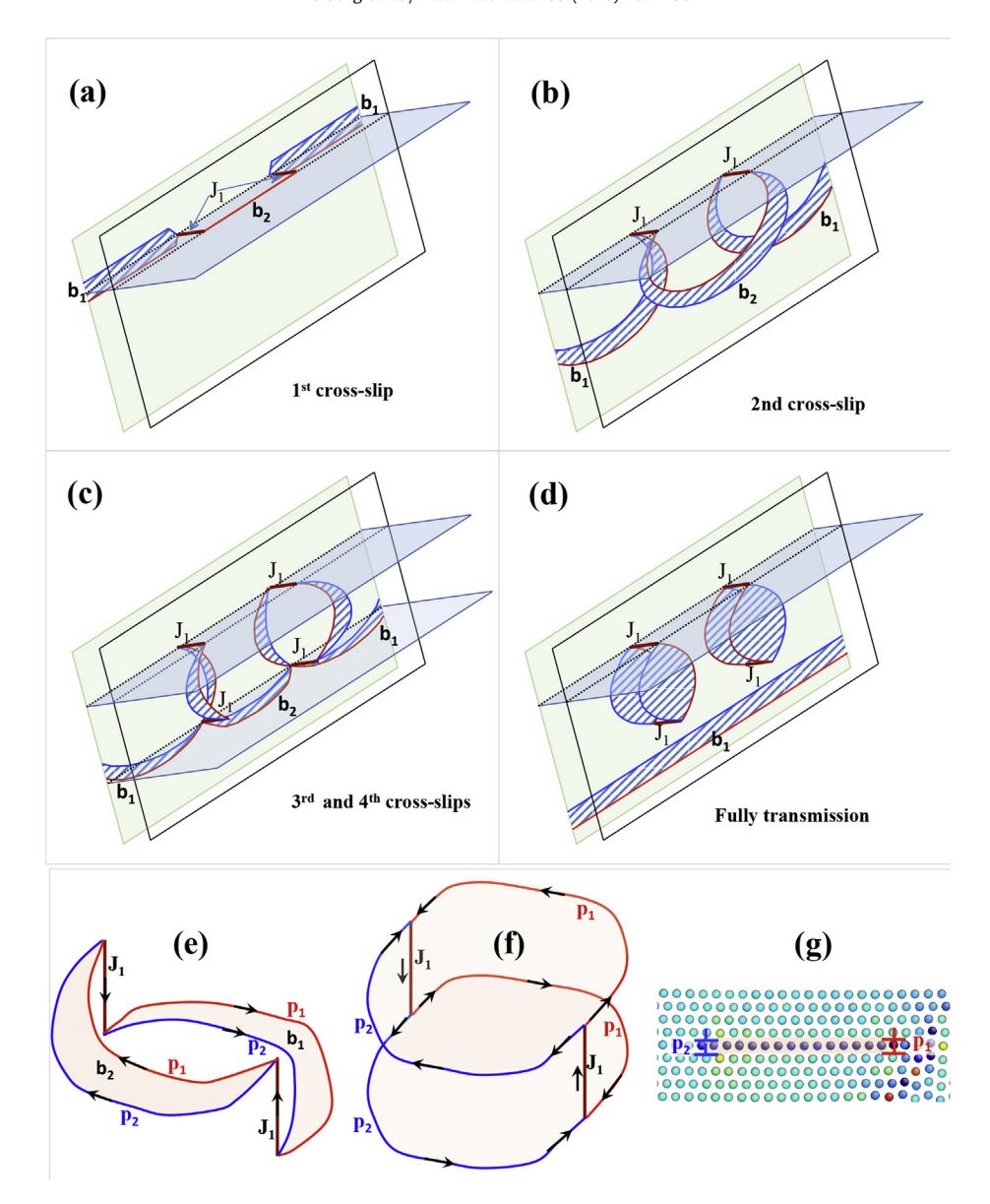


Fig. 6. Schematics of the interaction in case 1'. (a) Part of b_1 on basal plane crosses onto prismatic plane and becomes b_2 , leaving two J_1 . (b) b_2 on prismatic plane crosses onto adjacent basal plane. (c) Part of b_2 on adjacent basal plane crosses onto prismatic plane and then crosses onto origin basal plane, creating another two J_1 . (d) b_1 and b_2 on origin basal plane move as one and fully transform into twin, leaving two fault structures. (e) Close look at the dislocation configuration near J_1 in (c). (f) Close look at the dislocation configuration in (d). (g) Atomic configuration of the fault structure.

dislocation from the basal plane in the matrix onto the prismatic plane in the twin.

Case 4 An a_2 dislocation approaches the lateral-TB.

When the line of the a_2 dislocation is parallel to $[10\overline{1}0]$ on the basal plane, the dislocation is a 30° mixed type. The dislocation is initially placed 3 nm away from the lateral-TB. Under the applied deformation gradient F_2 , the twin propagates in the lateral direction and, simultaneously, the dislocation glides towards the twin and interacts with the lateral-TB. Fig. 11 shows the slip transformation processes. The key processes are analyzed in the following. First, the dislocation alters the propagation of the twin in the lateral direction. As shown in Fig. 11b, the two twin domains separated by the shear (or glide) plane of the incoming dislocation propagate with different speeds. As a consequence, a BP facet is created on the lateral side. Second, the continuous propagation of

the twin in the lateral direction is accompanied by the creation of a PSF due to the transformation and gliding of the a_2 dislocation on the prismatic plane of the twin, as shown in Fig. 11c. We characterized the prismatic stacking fault by the disregistry analysis [77] and attributed it to the shear associated with glide of $\frac{1}{2} < a_1 + c_2$ on prismatic planes. Correspondingly, the reaction of the a_2 dislocation crossing the twin can be described as

$$a_2(0001)_M \rightarrow \frac{1}{2} < a_1 + c > (10\overline{1}0)_T + \frac{1}{2}b^T$$

Thus, it is expected that a full $< a_1 + c >$ dislocation will be formed on the prismatic plane of the twin when two a_2 dislocations on the same basal plane in the matrix glide into the twin. We tested this idea by introducing two co-planar a_2 dislocations. Fig. 11d shows a full $< a_1 + c >$ dislocation in the twin without creating the PSF in the sheared region. The reaction can be described as

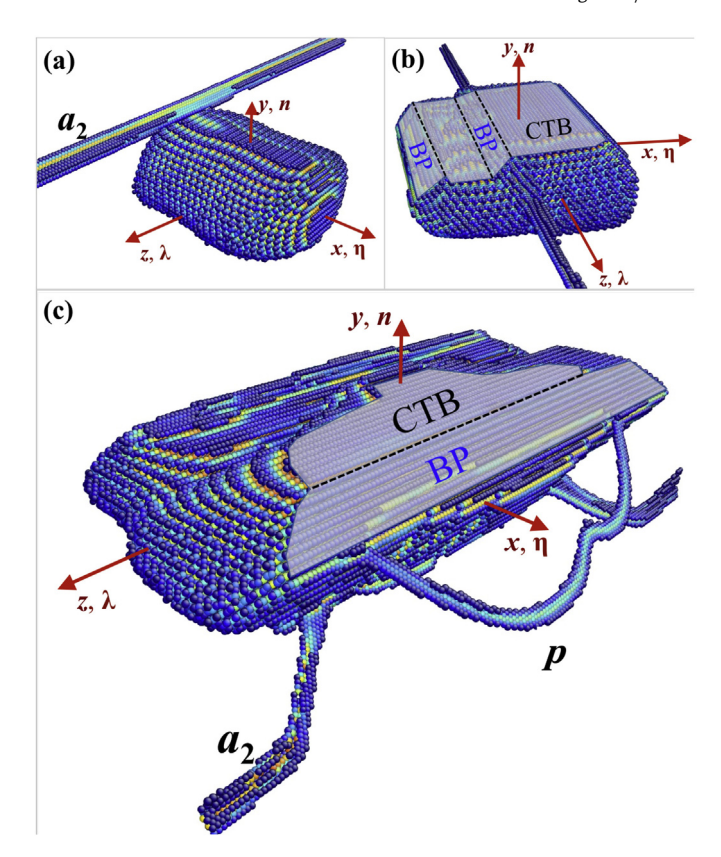


Fig. 7. (a) Initial atomic configuration of case 2 containing a twin and a mixed type a_2 dislocation. (b) Detwinning and formation of six-atomic-layer BP facet. (c) Final configuration showing obstruction of residual dislocation on normal-TB, transmutation of a_2 from lateral-TB and emission of basal dislocations from forward-TB.

$$2a_2(0001)_M \rightarrow \langle a_1 + c \rangle (10\overline{10})_T + b^r$$

The residual dislocation ${\bf b}^r$ has the magnitude $(\sqrt{1+k^2}-2)$ a=-0.09a for Mg, and can be smeared on the lateral-TB. It is worth mentioning that $2{\bf a}_2(0001)_M=<{\bf a}_1+{\bf c}>(10\overline{10})_T$ in a coherent PB interface, as discussed in Refs. [13–15,20,47,55]. Using atomistic simulation with empirical interatomic potential, we obtain a prismatic stacking fault energy of 308 mJ/m². Thus, the annihilation of the prismatic stacking fault in Fig. 8b and 8c can be explained by a reduction of the fault energy via nucleation of a partial dislocation loop with Burgers vector $\frac{1}{2}<{a}_1+{c}>(1010)_T$ in the faulted region.

The prediction of < c + a > dislocations is consistent with the experimental observations of < c + a > dislocations in the twin and near the boundary in Mg [15,20] and in Zn [14]. PSFs have been observed in Zr and Ti twins [54] but haven't been reported in Mg. Thus, the PSFs observed in the MD simulation could be an artifact of the energy profile associated with the shear on prismatic plane when using EAM/Liu's potential. To elucidate this question, we first calculated generalized stacking fault energy surface (γ -surface) of prismatic plane using molecular statics (MS) method with EAM/Liu's potential and with the modified-EAM (MEAM/Wu) potential [76]. Next, we compared the results with first-principles density function theory calculations.

In MS calculations, a single crystal model has the dimensions 1.60 nm (5a) in the $\begin{bmatrix} 11\overline{2}0 \end{bmatrix}$ direction (x-axis), 1.56 nm (3c) in the $\begin{bmatrix} 0001 \end{bmatrix}$ direction (z-axis), and 40 nm in the $\begin{bmatrix} 1\overline{1}00 \end{bmatrix}$ direction (y-axis). The periodic boundary condition is applied to the x- and z-axes. The γ -surface is obtained by shifting the half crystal with an

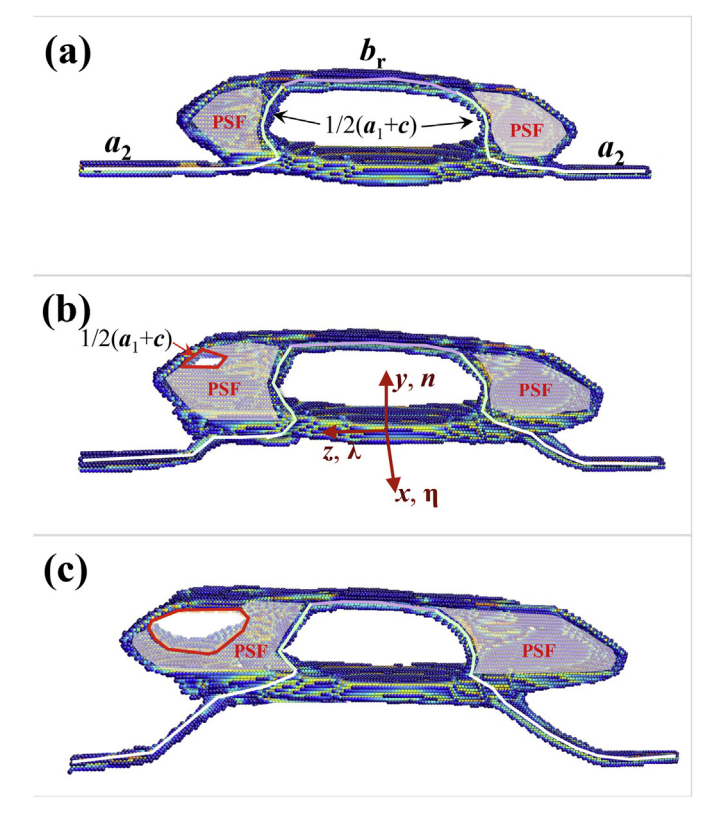


Fig. 8. (a) Transmutation of a_2 from matrix into twin as $\frac{1}{2} < a_1 + c_2$, creating prismatic stacking faults. Purple line depicts residual dislocation and white line depicts a_2 in matrix and $\frac{1}{2} < a_1 + c_2$ in twin. (b) and (c) Nucleation and migration of partial $\frac{1}{2} < a_1 + c_2$ loop on prismatic stacking faults. (For interpretation of the references to colour in this figure legend, the reader is referred to the Web version of this article.)

in-plane translation vector across the shear plane (prismatic plane), and then calculating the excess energy of the structure. During the relaxation, all the atoms are free to move along the

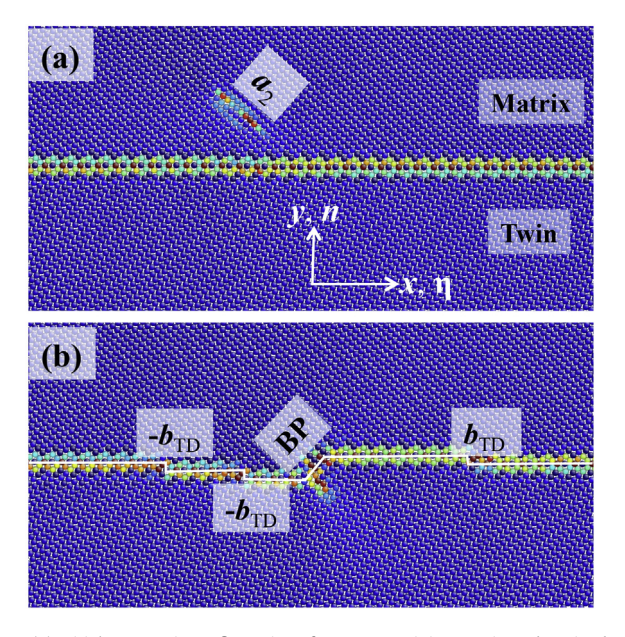


Fig. 9. (a) Initial 2D atomic configuration of case 2 containing a twin and a mixed type a_2 dislocation. (b) Dislocation dissociates on coherent twin boundary into three twinning dislocations and one residual dislocation. One six-atomic-layer BP facet forms during interaction.

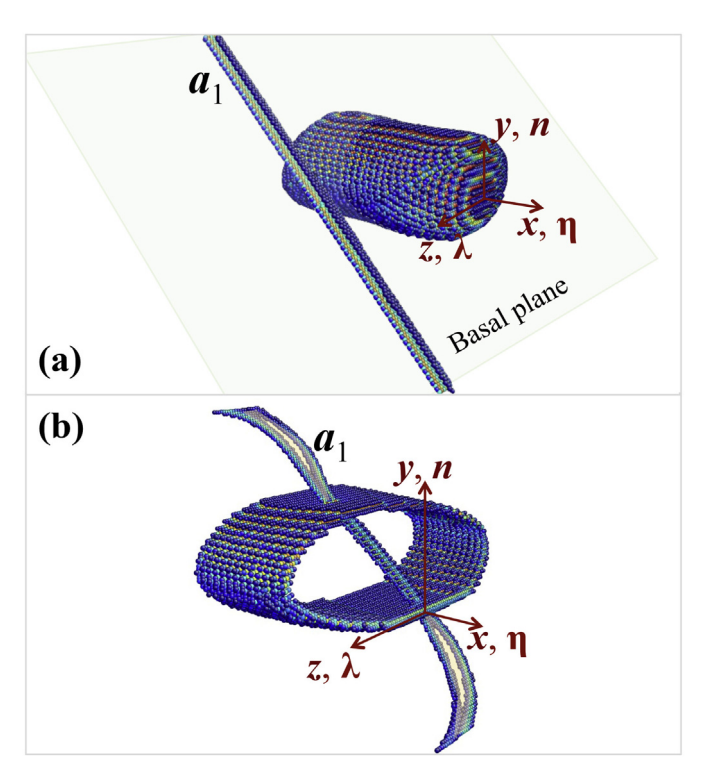


Fig. 10. (a) Initial atomic configuration of case 3 containing a twin and a pure edge a_1 dislocation. (b) Full transmutation of a_1 into twin.

normal direction of the shear plane but fixed along the two inplane directions to maintain the applied shear. In DFT calculation, the simulation model contains 40 atoms, and has the dimensions 0.3192 nm (1a) in the $\begin{bmatrix} 11\overline{2}0 \end{bmatrix}$ direction (x-axis), 0.5178 nm (1c) in the $\begin{bmatrix} 0001 \end{bmatrix}$ direction (z-axis), and 5.5287 nm (10 $\sqrt{3}a$) in the $\begin{bmatrix} 1\overline{1}00 \end{bmatrix}$ direction (y-axis). Periodic boundaries are adopted for both the x-axis and the z-axis, and two free surfaces along the y-axis are modeled by adding additional vacuum space. The γ -surface is computed by using the same calculation procedure as in the MS calculation. First principles density function

theory calculations were conducted using VASP.5.2. We used generalized gradient approximation (GGA) for the exchange correlation functional with the Perdew-Becke-Erzenhof (PBE) [85,86] parameterization, and projector augmented wave (PAW) pseudopotentials for the interaction between valence electrons and ionic cores [87]. The number of valence electrons in the pseudo-potentials are 2 (3 s2) for Mg [88]. We used a plane wave cutoff of 500 eV and $19 \times 19 \times 11$ Γ -centered Monkhorst Pack kpoint mesh for the integration of primitive hexagonal Brillouin zone (BZ) [89]. An optimized structure was obtained when the force on each atom is smaller than 0.0001 eV/nm. The optimized lattice parameters for Mg are a = 0.3192 nm and c = 0.5178 nm, giving c/a = 1.622, and -1.516 eV for the cohesive energy. We adopted $7 \times 1 \times 13$ Γ -centered Monkhorst Pack k-point mesh for the calculations of γ -surface. The convergence criterion of the structural relaxations and electronic self-consistency is that either the force acting on each atom is smaller than 10^{-5} eV/Å or the energy change between two steps is smaller than 10^{-5} eV.

Fig. 12 a-c show the generalized stacking fault energy surfaces calculated by EAM/Liu's and MEAM/Wu's empirical interatomic potentials, and the DFT. Notice that the three γ -surfaces show similar features, while MEAM/Wu's potential produces the highest stacking fault energy at the shear ½<a+c> on prismatic plane and EAM/Liu's potential produces the lowest stacking fault energy. Fig. 12d shows the variation of stacking fault energy along the $\langle a+c \rangle$ direction. It must be pointed out that both EAM/Liu's potential and DFT produce a local energy well at $\frac{1}{2} < a + c >$ (indicating that the PSF could be stable), while MEAM/Wu's potential does not. This difference could lead to different shear response on the prismatic plane. We thus tested this case with the MEAM/Wu's potential, Fig. 13a and 13b show two snapshots during the interaction between a single a_2 dislocation and the lateral-TB. Unsurprisingly, single a_2 dislocation did not transform into the twin, and the PSF observed in MD simulation with EAM/Liu's potential was not created in the twin. Moreover, Fig. 13c shows that slip transformation occurs via the formation and gliding of a full $\langle a_1 + c \rangle$ dislocation on the prismatic plane in the twin when two a_2 dislocation interact with the lateral-TB. The core of the $\langle a_1 + c \rangle$ dislocation is much narrower than that simulated with EAM/Liu's potential.

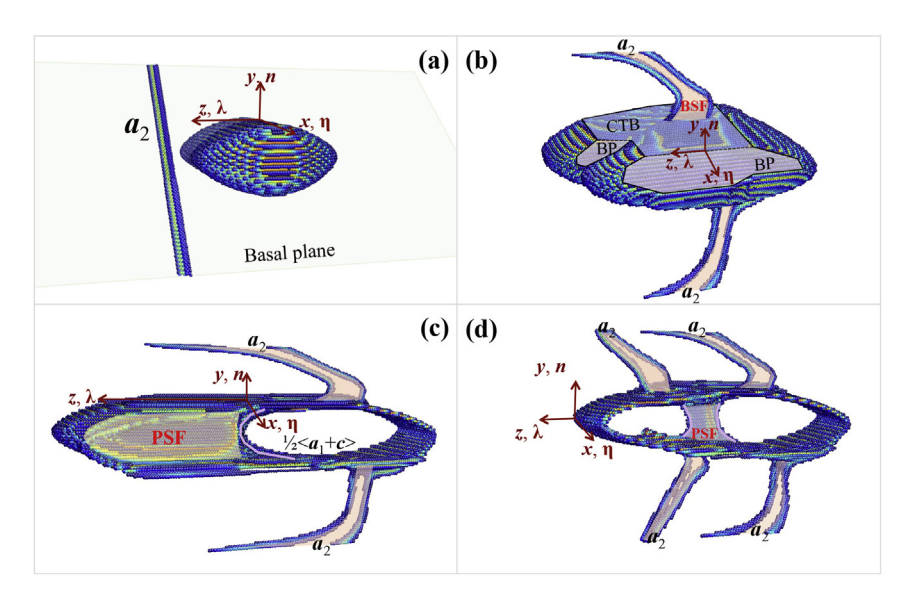


Fig. 11. (a) Initial atomic configuration of case 4 containing a twin and a mixed type a_2 dislocation. (b) a_2 fully transforms into twin, forming a BP facet on the shear plane of a_2 . (c) a_2 fully transmits into twin, creating prismatic stacking fault. (d) Transmutation of another a_2 on the same shear plane eliminates prismatic stacking fault.

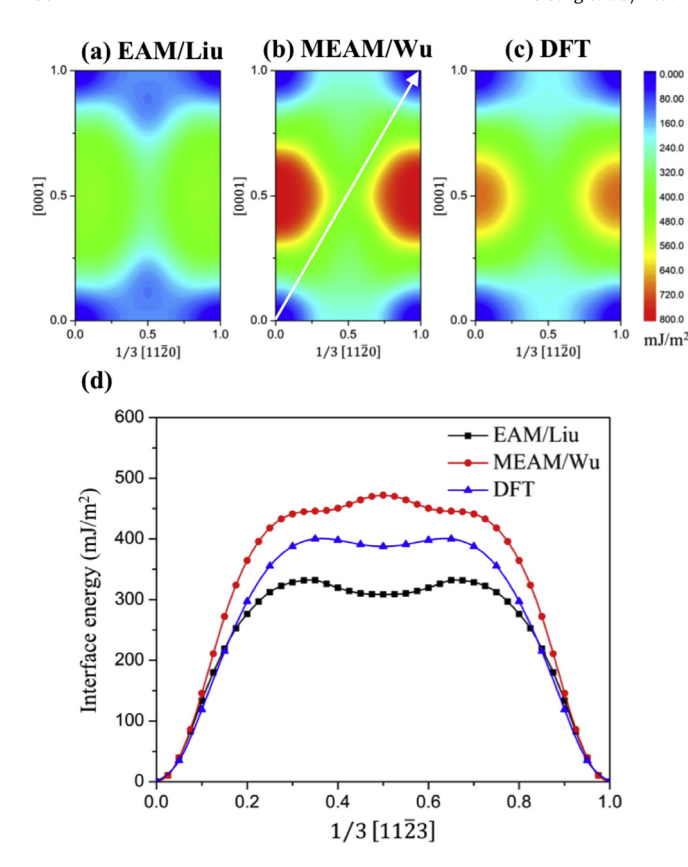


Fig. 12. Generalized stacking fault energy surface of prismatic plane, that are calculated with (a) EAM/Liu's potential, (b) MEAM/Wu's potential and (c) DFT. (d) Generalized stacking fault energy curves along < c+a > direction on prismatic plane.

4. Conclusions

Using atomistic simulations with empirical interatomic potential, we studied the interaction between basal <a> dislocations and a 3D twin for different dislocation characters and twin boundaries. The results provide insights into understanding slip transformation and dislocation reactions across twin boundaries, and the formation of basal and PSFs in the matrix and twin.

A dislocation with Burgers vector a_1 gliding on the basal plane of the matrix, can fully transform into the twin via cross-slip onto the prismatic plane in the twin and glide on the latter. In Mg, multiple cross-slip is observed via optical microscopy [22]. In Zr, with TEM characterization, both cross-slip from prismatic plane in the matrix onto prismatic plane in the twin and from prismatic plane in the matrix onto basal plane in the twin are frequently observed [50]. In Zn, direct transformation occurs, which is possibly related to the cross-slip [16,48]. Some differences are observed due to the different twin boundaries where the dislocation approaches. For example, fault structures may be generated during interaction between a_1 dislocation and a normal-TB. This gives a possible explanation of the BSFs near TBs [15,20,90].

• When a pure screw dislocation approaches the coherent twin boundary (cases 1 and 1'), the dislocation line may cross-slip from the original basal plane onto the prismatic plane in the matrix, then cross again onto the basal plane in the matrix, and finally transform into the twin and glide on the prismatic plane in the twin. Multiple cross-slip of the dislocation is driven by the local stress fields. This mechanism is a consequence of the 3D approach used here, and cannot be captured with a 2D approach. In addition, jogs with Burgers vector *a*₁ and aligned

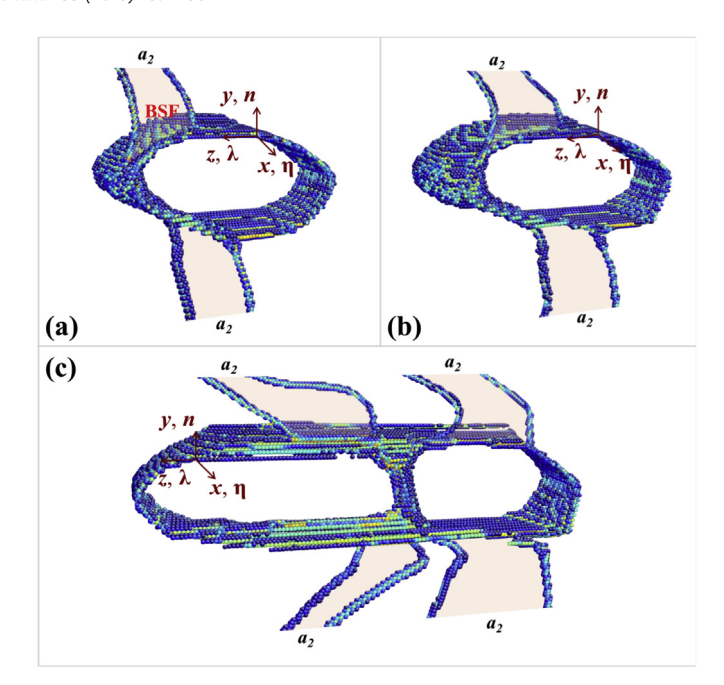


Fig. 13. Case 4 simulated with MEAM/Wu's potential. (a) and (b) Single a_2 dislocation does not transform into the twin. (c) Two a_2 dislocations transform into the twin through the glide of $< a_1 + c >$ dislocation on prismatic plane in the twin.

with the $<\!c\!>$ axis are formed accompanying the multiple cross-slip process. These jogs pin the dislocation line, causing either the formation of immobile dislocation configurations (basal stacking fault in Fig. 6) in the matrix or multiple prismatic a_1 dislocations left in the twin.

- When a pure edge dislocation approaches the lateral twin boundary (Case 3), the dislocation will directly transform into the twin from the basal plane in the matrix onto the prismatic plane in the twin.
- Mixed type dislocations on the basal plane with Burgers vector a₂ or a₃ (Case 2) cannot directly transformation across the coherent twin boundary. The dislocation line parallel to the coherent twin boundary will dissociate into twinning dislocations on the twin plane and a residual dislocation on the coherent twin boundary. This leads to a change in the twin thickness and the formation of a BP step associated with the gliding and pileup of twinning dislocations. The slip transformation might be accomplished through the gliding of ½<a₁+c> or <a₁+c> on the prismatic plane in the twin, provided the dislocation 'wraps around' the twin and reacts with the lateral boundary.
- When the dislocation line is of mixed character and approaches the lateral twin boundary (e.g. Case 4), the dislocation does not dissociate into twinning dislocations. The reaction processes show the dependence on the interatomic potentials. When the simulation is conducted with the EAM/Liu's potential, the dislocation transforms into the twin by the slip associated with gliding of a $\frac{1}{2} < a_1 + c >$ dislocation on the prismatic plane in the twin. As a consequence, PSFs are created in the twin. However, the transformation of a second a_2 or a_3 dislocation in the same plane erases the SF and the slip associated with the two dislocations is fully transformed into the twin by the gliding of a full $\langle a_1+c \rangle$ dislocation on the prismatic plane in the twin. When the simulation is conducted with the MEAM/Wu's potential, a single a_2 or a_3 dislocation does not transform into the twin, and the PSF predicted by the EAM/Liu's potential is not created in the twin. On the other hand, when two a_2 or a_3 dislocations impinge

on the lateral-TB, slip transformation occurs via the formation and gliding of a full $\langle a_1 + c \rangle$ dislocation on the prismatic plane in the twin. The difference in transformation processes between the two sets of simulations is ascribed to the prismatic stacking fault structure which is predicted by the two interatomic potentials. While the results indicate sensitivity of dislocation reactions to detailed properties of the potentials involved, it is encouraging that either result is at present consistent with experimental data.

 Once again, some of these processes can only be captured by a 3D simulation.

The work described above predicts the formation of dislocation structures inside twins and at twin interfaces, following dislocation-twin interaction and possible transformation into the twin. A highlight of this work is that the atomistic predictions suggest that the results of these reactions can be fairly complex dislocation structures. For example, the creation of a PSF accompanies the gliding of $\frac{1}{2} < a_1 + c_2$ dislocations. The prediction of $< c + a_2$ dislocations is consistent with the experimental observations of $< c + a_2$ dislocations inside the twin near the boundary in Mg [15,20] and in Zn [14]. PSFs are observed in Zr and Ti twins [54] but haven't been reported in Mg. In Mg, PSF could be stable with a limited size. It will eventually be annihilated via the nucleation of a partial loop in the faulted region because of its high stacking fault energy.

Therefore, 3D atomistic simulation complements the geometric/ crystallographic analysis [10-12,55,91] and provides a comprehensive understanding of dislocation-twin interactions. The Correspondence Matrix Rule (CMR), understood as the crystallographic transformation of the dislocation line and Burgers vector taking place as a consequence of the twin reorientation, was introduced by Bilby [92] and applied to HCP twins by Yoo [93] and Niewczas [91]. Previous 2D atomistic simulations done by El Kadiri et al. [41], indicate already that CMR may not capture the complicated processes revealed by atomistic calculations. Different and complex reactions could take place depending on local atomic structure of the interface, temperature, and local stress field. The reactions at the twin interface are more likely than not to produce residual dislocations that get trapped at or in the vicinity of the interface, plus dissociations into partials that may be able to glide inside the twin domain. In our view, atomistic simulations, guided and supported by TEM characterization, need to be used for inferring these processes.

Acknowledgments

This work was fully funded by the U.S. Dept. of Energy, Office of Basic Energy Sciences Project FWP 06SCPE401. MG and GL were funded by the aforementioned Project through Contract LANS RFP No. 364175 Mod 2. JW also acknowledge supports from the US National Science Foundation (NSF) (CMMI-1661686). Atomistic simulations were completed utilizing the Holland Computing Center of the University of Nebraska, which receives support from the Nebraska Research Initiative.

References

- P.G. Partridge, The crystallography and deformation modes of hexagonal close-packed metals, Metall. Rev. 12 (1967) 169–194.
- [2] M.H. Yoo, C.T. Wei, Slip modes of hexagonal-close-packed metals, J. Appl. Phys. 38 (1967) 4317–4322.
- [3] J.W. Christian, S. Mahajan, Deformation twinning, Prog. Mater. Sci. 39 (1995) 1–157
- [4] P.W. Bakarian, C.H. Mathewson, Slip and twinning in Magnesium single crystals at elevated temperatures, Transactions of the Metallurgical Society of AIME 152 (1943) 226–254.

- [5] J. Morris, K. Ho, K. Chen, G. Rengarajan, M. Yoo, Large-scale atomistic study of core structures and energetics of dislocations in hexagonal close packed metals, Model. Simulat. Mater. Sci. Eng. 8 (2000) 25.
- [6] S. Zhou, A. Carlsson, R. Thomson, Dislocation core-core interaction and Peierls stress in a model hexagonal lattice, Phys. Rev. B 49 (1994) 6451.
- [7] Y. Chou, Interaction of parallel dislocations in a hexagonal crystal, J. Appl. Phys. 33 (1962) 2747–2751.
- [8] N. Bertin, C.N. Tomé, I.J. Beyerlein, M.R. Barnett, L. Capolungo, On the strength of dislocation interactions and their effect on latent hardening in pure Magnesium, Int. J. Plast. 62 (2014) 72–92.
- [9] L. Capolungo, Dislocation junction formation and strength in magnesium, Acta Mater. 59 (2011) 2909—2917.
- [10] A.W. Sleeswyk, C.A. Verbraak, Incorporation of slip dislocations in mechanical twins—I, Acta Metallurgica 9 (1961) 917—927.
- [11] M.H. Yoo, Interaction of slip dislocations with twins in hcp metals, Transactions of the Metallurgical Society of AIME 245 (1969), 2061–2060.
- [12] I. Saxl, The incorporation of slip dislocations in twins, Czech. J. Phys. 18 (1968) 39–49
- [13] D.M. Vallance, M. Bevis, The interaction of slip dislocations with twin boundaries, Scripta Mater. 4 (1970) 681–684.
- [14] D.I. Tomsett, M. Bevis, The incorporation of basal slip dislocations in {1012} twins in zinc crystals, Phil. Mag. 19 (1969) 129–140.
- [15] S. Morozumi, M. Kikuchi, H. Yoshinaga, Electron microscope observation in and around (1-102) twins in magnesium, Transactions of Janpan Institute of Metals 17 (1976) 158–164.
- [16] S. Lay, G. Nouet, Interaction of slip dislocations with the (0112) twin interface in zinc, Philos. Mag. a 70 (1994) 1027–1044.
- [17] A. Serra, D.J. Bacon, Computer simulation of screw dislocation interactions with twin boundaries in HCP metals, Acta Metall. Mater. 43 (1994) 4465–4481.
- [18] J. Wang, I.J. Beyerlein, C.N. Tomé, Reactions of lattice dislocations with grain boundaries in Mg: implications on the micro scale from atomic-scale calculations, Int. J. Plast. 56 (2014) 156–172.
- [19] J. Zhang, G. Xi, X. Wan, C. Fang, The dislocation-twin interaction and evolution of twin boundary in AZ31 Mg alloy, Acta Mater. 133 (2017) 208–216.
- [20] F. Wang, S.R. Agnew, Dislocation transmutation by tension twinning in magnesium alloy AZ31, Int. J. Plast. 81 (2016) 63–86.
- [21] H. El Kadiri, A.L. Oppedal, A crystal plasticity theory for latent hardening by glide twinning through dislocation transmutation and twin accommodation effects, J. Mech. Phys. Solid. 58 (2010) 613–624.
- [22] K.D. Molodov, T. Aİ-Samman, D.A. Molodov, Profuse slip transmission across twin boundaries in magnesium, Acta Mater. 124 (2017) 397–409.
- [23] L. Capolungo, I.J. Beyerlein, G.C. Kaschner, C.N. Tomé, On the interaction between slip dislocations and twins in HCP Zr, Mater. Sci. Eng., A 513–514 (2009) 42–51.
- [24] M.S. Hooshmand, M.J. Mills, M. Ghazisaeidi, Atomistic modeling of dislocation interactions with twin boundaries in Ti, Model. Simulat. Mater. Sci. Eng. 25 (2017), 045003.
- [25] H. Fan, S. Aubry, A. Arsenlis, J.A. El-Awady, The role of twinning deformation on the hardening response of polycrystalline magnesium from discrete dislocation dynamics simulations, Acta Mater. 92 (2015) 126–139.
- [26] A. Jain, S.R. Agnew, Modeling the temperature dependent effect of twinning on the behavior of magnesium alloy AZ31B sheet, Mater. Sci. Eng., A 462 (2007) 29–36.
- [27] G. Proust, C.N. Tomé, A. Jain, S.R. Agnew, Modeling the effect of twinning and detwinning during strain-path changes of magnesium alloy AZ31, Int. J. Plast. 25 (2009) 861–880.
- [28] H. El Kadiri, J. Kapil, A.L. Oppedal, L.G. Hector, S.R. Agnew, M. Cherkaoui, S.C. Vogel, The effect of twin—twin interactions on the nucleation and propagation of twinning in magnesium, Acta Mater. 61 (2013) 3549—3563.
- [29] B.M. Morrow, E.K. Cerreta, R.J. McCabe, C.N. Tome, Toward understanding twin—twin interactions in hcp metals: utilizing multiscale techniques to characterize deformation mechanisms in magnesium, Mater. Sci. Eng., A 613 (2014) 365–371.
- [30] B.M. Morrow, R.J. McCabe, E.K. Cerreta, C.N. Tomé, Observations of the atomic structure of tensile and compressive twin boundaries and twin—twin interactions in zirconium, Metall. Mater. Trans. 45 (2014) 5891–5897.
- [31] Q. Yu, J. Wang, Y. Jiang, R.J. McCabe, N. Li, C.N. Tomé, Twin—twin interactions in magnesium, Acta Mater. 77 (2014) 28–42.
- [32] Q. Yu, J. Zhang, Y. Jiang, Direct observation of twinning-detwinning-retwinning on magnesium single crystal subjected to strain-controlled cyclic tension-compression in [0 0 0 1] direction, Phil. Mag. Lett. 91 (2011) 757-765.
- [33] J. Wang, Q. Yu, Y. Jiang, I.J. Beyerlein, Twinning-associated boundaries in hexagonal close-packed metals, JOM (J. Occup. Med.) 66 (2013) 95–101.
- [34] S. Xu, M. Gong, C. Schuman, J.-S. Lecomte, X. Xie, J. Wang, Sequential (10-12) twinning stimulated by other twins in titanium, Acta Mater. 132 (2017) 57–68
- [35] S. Xu, M. Gong, X. Xie, Y. Liu, C. Schuman, J.-S. Lecomte, J. Wang, Crystallo-graphic characters of {1122} twin-twin junctions in titanium, Phil. Mag. Lett. (2017) 1–13.
- [36] A. Berghezan, A. Fourdeux, S. Amelinckx, Transmission electron microscopy studies of dislocations and stacking faults in a hexagonal metal: Zinc, Acta Metallurgica 9 (1961) 464–490.
- [37] G. Proust, C. Tomé, G. Kaschner, Modeling texture, twinning and hardening

- evolution during deformation of hexagonal materials, Acta Mater, 55 (2007) 2137-2148.
- [38] Q. Yu, J. Wang, Y. Jiang, R.J. McCabe, C.N. Tomé, Co-zone {-1012} twin interaction in magnesium single crystal, Materials Research Letters 2 (2014) 82-88
- [39] Q. Yu, Y. Jiang, J. Wang, Cyclic deformation and fatigue damage in singlemagnesium under fully reversed crystal strain-controlled tension—compression in the [10-10] direction, Scripta Mater. 96 (2015) 41-44
- [40] A. Serra, D.J. Bacon, R.C. Pond, Twins as barriers to basal slip in hexagonalclose-packed metals, Metall, Mater, Trans, 33 (2002) 809-812.
- [41] H. El Kadiri, C.D. Barrett, J. Wang, C.N. Tomé, Why are {10-12} twins profuse in magnesium? Acta Mater. 85 (2015) 354-361.
- [42] M. Arul Kumar, A.K. Kanjarla, S.R. Niezgoda, R.A. Lebensohn, C.N. Tomé, Numerical study of the stress state of a deformation twin in magnesium. Acta Mater, 84 (2015) 349-358.
- [43] A. Fernandez, A. Jérusalem, I. Gutiérrez-Urrutia, M. Pérez-Prado, 3D investigation of the grain boundary-twin interactions in a Mg AZ31 alloy by 3D EBSD and continuum modeling, Acta Mater. 61 (2013) 7679–7692.
- Y. Liu, N. Li, S. Shao, M. Gong, J. Wang, R.J. McCabe, Y. Jiang, C.N. Tome, Characterizing the boundary lateral to the shear direction of deformation twins in magnesium, Nat. Commun. 7 (2016) 11577.
- [45] M. Gong, J.P. Hirth, Y. Liu, Y. Shen, J. Wang, Interface structures and twinning mechanisms of twins in hexagonal metals, Mater Res Lett (2017) 1-16.
- [46] A. Luque, M. Ghazisaeidi, W.A. Curtin, A new mechanism for twin growth in Mg alloys, Acta Mater. 81 (2014) 442–456.
- [47] D.I. Tomsett, M. Bevis, The formation of stacking faults in {1012} twins in zinc as a result of slip dislocation-deformation twin interactions, Phil. Mag. 19 (1969) 533-537.
- [48] P.B. Price, Nucleation and growth of twins in dislocation-free zinc, in proceedings of the Royal Society of London a Mathematical, Physical and Engineering Sciences 260 (1961) 251-262.
- [49] R.E. Cooper, J. Washburn, Stress-induced movement of twin boundaries in zinc, Acta Metall. 15 (1967) 639-647.
- [50] J.I. Dickson, C. Robin, The incorporation of slip dislocations in {1-102} twins in zirconium, Mater. Sci. Eng. 11 (1973) 299-302.
- [51] D.G. Westlake, Twinning in zirconium, Acta Metall. 9 (1961) 327-331.
- [52] F.C. Frank, LXXXIII. Crystal dislocations.—elementary concepts and definitions, The London, Edinburgh, and Dublin Philosophical Magazine and Journal of Science 42 (1951) 809-819.
- [53] D. Bhattacharyya, E.K. Cerreta, R. McCabe, M. Niewczas, G.T. Gray, A. Misra, C.N. Tomé, Origin of dislocations within tensile and compressive twins in pure textured Zr, Acta Mater. 57 (2009) 305-315.
- S.G. Song, G.T. Gray, Structural interpretation of the nucleation and growth of deformation twins in Zr and Ti-II. Tem study of twin morphology and defect reactions during twinning, Acta Metall. Mater. 43 (1995) 2339–2350.
- [55] M.H. Yoo, C.T. Wei, Growth of deformation twins in zinc crystals, Phil. Mag. 14 (1966) 573-587.
- [56] A. Serra, D.J. Bacon, R.C. Pond, Dislocations in interfaces in the hcp metals—I. Defects formed by absorption of crystal dislocations, Acta Mater. 47 (1999) 1425-1439.
- [57] A. Serra, D.J. Bacon, A new model for {10-12} twin growth in hcp metals, Philos. Mag. a 73 (1996) 333-343.
- [58] J. Wang, I.J. Beyerlein, J.P. Hirth, Nucleation of elementary {-1011} and {-1013} twinning dislocations at a twin boundary in hexagonal close-packed crystals, Model. Simulat. Mater. Sci. Eng. 20 (2012) 024001.
- [59] J. Wang, L. Liu, C.N. Tomé, S.X. Mao, S.K. Gong, Twinning and de-twinning via glide and climb of twinning dislocations along serrated coherent twin boundaries in hexagonal-close-packed metals, Mater Res Lett. 1 (2013)
- [60] I. Shin, E.A. Carter, Simulations of dislocation mobility in magnesium from first principles, Int. J. Plast. 60 (2014) 58-70.
- [61] S. Groh, E.B. Marin, M.F. Horstemeyer, D.J. Bammann, Dislocation motion in magnesium: a study by molecular statics and molecular dynamics, Model. Simulat. Mater. Sci. Eng. 17 (2009) 075009.
- [62] R. Lebensohn, C. Tomé, A study of the stress state associated with twin nucleation and propagation in anisotropic materials, Philos. Mag. a 67 (1993)
- [63] A. Ostapovets, A. Serra, Characterization of the matrix-twin interface of a (1012) twin during growth, Philos. Mag. A 94 (2014) 2827–2839.
- [64] A. Ostapovets, R. Gröger, Twinning disconnections and basal-prismatic twin

- boundary in magnesium, Model. Simulat. Mater. Sci. Eng. 22 (2014).
- [65] A. Ostapovets, A. Serra, Evolution of matrix-twin interfaces of (1012) twin in magnesium, Acta Phys. Pol., a 128 (2015) 661-664.
- [66] C.D. Barrett, H. El Kadiri, The roles of grain boundary dislocations and disclinations in the nucleation of {102} twinning, Acta Mater. 63 (2014) 1–15.
- [67] C.D. Barrett, H. El Kadiri, Impact of deformation faceting on {10-12}, {10-11} and {10-13} embryonic twin nucleation in hexagonal close-packed metals. Acta Mater. 70 (2014) 137–161.
- [68] J. Wang, S.K. Yadav, J.P. Hirth, C.N. Tomé, I.I. Beverlein, Pure-shuffle nucleation of deformation twins in hexagonal-close-packed metals, Materials Research Letters 1 (2013) 126-132.
- [69] B.-Y. Liu, J. Wang, B. Li, L. Lu, X.Y. Zhang, Z.-W. Shan, J. Li, C.-L. Jia, J. Shu, E. Ma, Twinning-like lattice reorientation without a crystallographic twinning plane, Nat Commun 5 (2014)
- [70] B. Xu, L. Capolungo, D. Rodney, On the importance of prismatic/basal interfaces in the growth of twins in hexagonal close packed crystals, Scripta Mater 68 (2013) 901-904
- [71] J. Wang, I.J. Beyerlein, C.N. Tomé, An atomic and probabilistic perspective on
- twin nucleation in Mg, Scripta Mater. 63 (2010) 741–746.

 [72] J. Wang, J.P. Hirth, C.N. Tomé, (-1012) Twinning nucleation mechanisms in hexagonal-close-packed crystals, Acta Mater. 57 (2009) 5521-5530.
- [73] J. Wang, I.J. Beyerlein, J.P. Hirth, C.N. Tomé, Twinning dislocations on {-1011} and {-1013} planes in hexagonal close-packed crystals, Acta Mater. 59 (2011) 3990-4001
- [74] D.M. Barnett, J. Lothe, An image force theorem for dislocations in anisotropic bicrystals, J. Phys. F Met. Phys. 4 (1974) 1618.
- [75] X.-Y. Liu, J. Adam, F. Ercolessi, J. Moriarty, EAM potential for magnesium from quantum mechanical forces, Model. Simulat. Mater. Sci. Eng. 4 (1996) 293.
- [76] Z. Wu, M.F. Francis, W.A. Curtin, Magnesium interatomic potential for simulating plasticity and fracture phenomena, Model. Simulat. Mater. Sci. Eng. 23 (2015)
- [77] J.P. Hirth, J. Lothe, Theory of Dislocations, second ed., Wiley, New York, 1982.
- [78] A. Serra, R.C. Pond, D.J. Bacon, Computer simulation of the structure and mobility of twinning dislocations in hcp metals, Acta Metall, Mater. 39 (1991) 1469-1480
- [79] A. Serra, D.J. Bacon, R.C. Pond, The crystallography and core structure of twinning dislocations in hcp metals, Acta Metall. 36 (1988) 3183-3203.
- [80] J.P. Hirth, R.C. Pond, Steps, dislocations and disconnections as interface defects relating to structure and phase transformations, Acta Mater. 44 (1996) 4749-4763.
- [81] J.P. Hirth, J. Wang, C.N. Tomé, Disconnections and other defects associated with twin interfaces, Prog. Mater. Sci. 83 (2016) 417-471.
- [82] R.C. Pond, A. Serra, A.P. Sutton, The crystallography and atomic structure of line defects in twin boundaries in hexagonal-close-packed metals, Metall. Mater. Trans. 22 (1991) 1185-1196.
- [83] J. Wang, Y. Shen, Structure-property-functionality Relationships in bimetal composites, JOM (J. Occup. Med.) 64 (2012) 1190-1191.
- H.A. Khater, A. Serra, R.C. Pond, Atomic shearing and shuffling accompanying the motion of twinning disconnections in Zirconium, Phil. Mag. 93 (2013) 1279-1298.
- [85] G. Kresse, J. Hafner, Ab initio molecular dynamics for liquid metals, Phys. Rev. B 47 (1993) 558.
- [86] J.P. Perdew, J.A. Chevary, S.H. Vosko, K.A. Jackson, M.R. Pederson, D.J. Singh, C. Fiolhais, Atoms, molecules, solids, and surfaces: applications of the generalized gradient approximation for exchange and correlation, Phys. Rev. B 46 1992) 6671.
- [87] G. Kresse, J. Furthmüller, Efficiency of ab-initio total energy calculations for metals and semiconductors using a plane-wave basis set, Comput. Mater. Sci. 6 (1996) 15-50.
- [88] G. Kresse, J. Hafner, Norm-conserving and ultrasoft pseudopotentials for firstrow and transition elements, J. Phys. Condens. Matter 6 (1994) 8245.
- [89] J.P. Perdew, Unified theory of exchange and correlation beyond the local density approximation, Electronic structure of solids 91 (11) (1991).
- [90] J. Tu, X. Zhang, J. Wang, Q. Sun, Q. Liu, C.N. Tomé, Structural characterization of (10-12) twin boundaries in cobalt, Appl. Phys. Lett. 103 (2013) 051903.
- [91] M. Niewczas, Lattice correspondence during twinning in hexagonal closepacked crystals, Acta Mater. 58 (2010) 5848-5857.
- [92] B.A. Bilby, A. Crocker, The theory of the crystallography of deformation twinning, Proc. Roy. Soc. Lond. A 288 (1965) 240-255
- [93] M. Yoo, Slip, twinning, and fracture in hexagonal close-packed metals, Metallurgical Transactions A 12 (1981) 409-418.